Structural, thermal behaviour and vibrational study of a new mixed cesium–ammonium tellurate

WAFA BEN ARIBIA[a], MAKKI ABDELMOULEH[a], VAN DER LEE[b]
and AHLEM KABADOU[a,*]

[a]Laboratoire de Sciences des Matériaux et de l'environnement, Faculté des Sciences de Sfax, Université de Sfax, BP 1171, 3000 Sfax, Tunisia
[b]Institut Européen des Membranes (UMR 5635), Université de Montpellier II, cc 047, Place E. Montpellier, France
e-mail: ahlemkabadou@yahoo.fr

Abstract. Synthesis, crystal structure, thermal characterization, FTIR and Raman measurements are given for a new mixed compound cesium–ammonium tellurate. X-ray study showed that the $[Cs_{0.92}(NH_4)_{0.08}]_2TeCl_4Br_2$ compound crystallizes in the tetragonal space group P4/mnc, with a = 7.452 (1) Å, c = 10.544 (3) Å and Z = 2. The refinement converged at room temperature to $R_p = 0.093$ and $R_{wp} = 0.076$. The structure is considered as isolated octahedral $TeCl_4Br_2^{2-}$. These anions show a 4° rotation around the fourfold axis against the cubic arrangement of the K_2PtCl_6 type structure. The monovalent cations (Cs^+/NH_4^+) are located between the octahedra ensuring the stability of the structure by ionic and hydrogen bonding contacts: Cs...Cl/Br and N-H......Cl/Br. A DTA/TGA experiment at high temperature reveals one endothermic peak at 780 K for this compound. At low temperature a transition from phase I to phase II was detected at 213 K by DSC. This transition, confirmed by Raman analysis, can be attributed to an order–disorder phase transition.

Keywords. Crystal growth; X-ray diffraction; crystal structure; Raman spectroscopy.

1. Introduction

In 1957, Gillespie and Nyholm[1] developed the valence shell electron-pair repulsion theory, according to which the lone pair of electrons present in, for example, the hexachlorotellurate(IV) complex anion should be stereochemically active and distort the coordination polyhedron from being regular octahedral.

The structure of tellurium materials has been extremely popular in recent years due to the peculiar electronic configurations of tellurium IV, whose electron lone pair induces several coordinations and unusual structures.[2–4]

However, The A_2TeX_6 family (A being alkali metal and X a halogen) represents also a vast class of semiconductors. They have been attracting considerable attention because of their potential applications in optical modulation and scanning devices.[5]

For compounds A_2TeBr_6 (with A = K, NH_4, Rb, Cs)[6–8] the high-temperature phases show the cubic K_2PtCl_6 type structure. Lowering the temperature, second order phase transitions can be observed, especially when the anions are comparatively large. These phase transitions can be explained by a softening of rotary phonons. Generally, in A_2MX_6 compounds this instability is a result of a double minimum in the Coulomb potential with respect to the octahedra tilt angle φ around (0 0 1); the depth of this minimum depends on the interaction study[9] which give us a hint for understanding the lattice dynamics of A_2MX_6 phases.

For investigating the sample dynamics, the degree of disorder in the different phases and the mechanisms involved in the transition with temperature, Raman scattering provides a powerful tool. Raman scattering measurements on $[Cs_{0.92}(NH_4)_{0.08}]_2TeCl_4Br_2$ material taken between 120 K and 400 K are reported in this paper.

2. Experimental

2.1 *Synthesis of sample and characterization*

Tellurium dioxide (TeO_2) was dissolved in the minimum amount of concentrated hydrochloric acid by heating. Two separate solutions of ammonium bromide and cesium bromide were prepared, then slowly and simultaneously added to the first solution (if a

precipitate formed, it was reheated until dissolution). A few drops of concentrated hydrochloric acid were added to the hot solution until there was a permanent precipitate. The new mixed powder was filtered and stored in a desiccator containing a small beaker of potassium hydroxide pellets in addition to silica gel. The formula of this compound is determined by chemical analysis (table 1) and confirmed by refinement of the structure using the Rietveld method.

2.2 *X-ray studies*

The sample was mounted in the toploaded sample holder and investigated by X-ray powder diffraction (XRD). These samples were mounted in the top-loaded sample holders and investigated by X-ray powder diffraction technique (XRD). Powder X-ray diffraction data were collected at room temperature using a PANalytical X'pert-Pro diffractometer equipped with an ultrafast X'celerator detector. Ni-filtered Cu K_α X-ray (40 kV/40 mA) were used. In order to limit the axial divergence, 0.02 rad primary and secondary Soller slits were inserted. Data were collected by continuous scan from 10 to 120° 2θ with an effective step size of 0.016 and 20 s integration time per step. It is noted that the position sensitive X'celerator detector has an opening angle of 2.122° with 127 channels. Prior to data analysis, the experimental data were recalculated to step sizes of 0.016° using a cubic spline interpolation method. Indexing was performed using DICVOL04 software[10] with standard options confidence factors of M(20) = 41 and F(20) = 33.8.[11] Our assumption was subsequently confirmed by successful Rietveld refinement of the investigated structure.

The X-ray powder diffraction data were refined by the Rietveld method[12] using the FULLPROF code.[13] The Rietveld refinement was carried out using the pseudo-Voigt function[14] for the simulation of the peak shapes. Le Bail profile refinement was first used to find the profile and instrumental parameters such as the zero-angle displacement error and asymmetry effects. The background was fitted with a linear interpolation between the 30 given points.[15] The refinement with halfwidth parameters U, V, W, unit cell parameters mixing coefficient and the symmetry parameters converged to $\chi^2 = 0.059$. Then, the assumed structure was refined while fixing the profile and instrumental parameters. The refinement of Br and Cl in the same positions diverges and is not stable. For this reason, the Cl and Br atoms are fixed in two different positions and then they are ordered.

A final refinement taking into account the overall isotropic displacement factor (Bov) converged to $R_P = 0.093$, $R_{wp} = 0.076$, and $R_{bragg} = 0.018$ (table 2). Low values of the profile residuals, Rp and Rwp, indicate a high background level rather than the real profile agreement, but low R_B values (which are not affected by the background level) show the reasonable agreement between the experimental and theoretical structural models. The occupancy probability of the Cs and N atoms was refined in such a way that the total occupancy was equal to 1 (table 3).

Crystal structure data and experimental conditions are collected in table 2. Positional and isotropic thermal parameters of the ternary halides $[Cs_{0.92}(NH_4)_{0.08}]_2$ $TeCl_4Br_2$ are summarised in table 3. Figure 1 illustrates the final Rietveld plots for $[Cs_{0.92}(NH_4)_{0.08}]_2TeCl_4Br_2$.

Table 1. Results of chemical analysis for $[Cs_{0.92}(NH_4)_{0.08}]_2TeCl_4Br_2$.

	Te (%)	Cl (%)	Br (%)	N (%)	Cs (%)
Calculated	18.85	20.96	23.62	0.42	36.15
Experimental	19.11[a]	20.25[b]	23.72[b]	0.48[c]	37.23[d]

[a]Determined gravimetrically by reduction with (SO$_2$) to the element Te.[20]
[b]Determined by potentiometric method.
[c]Determined by a Kjeldahl apparatus method.
[d]Determined using a flame photometer.

Table 2. Crystal structure data and experimental conditions of structure determination of $[Cs_{0.92}(NH_4)_{0.08}]_2TeCl_4Br_2$.

Formula	$[Cs_{0.92}(NH_4)_{0.08}]_2TeCl_4Br_2$
Temperature (K)	293
Space group	*P4/mnc*
a (Å)	7.452(1)
c (Å)	10.5440 (3)
V(Å^3)	585.5652(3)
Z	2
D_x (gcm^{-3})	3.83
Radiation (Å)	Cu(K$_{\alpha1}$) = 1.54060, Cu(K$_{\alpha2}$) = 1.54433
Diffractometer	PANalytical X'pert-Pro
2θ range of refinement (°)	10 – 120
Number of structural variables[a]	7
Number of global parameters[b]	38
R_P	0.093
R_{wp}	0.076
χ^2	0.059
R_{bragg}	0.018

[a]Including the scale factor.
[b]Including background coefficients, cell parameters, Pseudo–Voigt function parameters, and asymmetry parameters.

Table 3. Positional equivalent and isotropic thermal parameters for the structure of $[Cs_{0.92}(NH_4)_{0.08}]_2TeCl_4Br_2$.

Atoms	Site	x	y	z	B_{iso} (Å^2)	Occ. factor
$[Cs_{0.92}(NH_4)_{0.08}]_2TeCl_4Br_2$						
Te	2b	1/2	1/2	0	0.52951	1
Cs	4d	0	1/2	1/4	1.78147(10)	0.920(4)
N	4d	0	1/2	1/4	1.78147(10)	0.080(4)
Br	4e	0	0	0.2518(1)	0.7206(13)	1
Cl	8h	0.7639(4)	0.2733(8)	0	0.3232(8)	1
H	16i	0	0.4380	0.1800	0.82744	0.020

2.3 *Thermal behaviour*

DTA/TGA measurements were carried out on 5–10 mg samples at a heating rate of 10 K.min^{-1} using a Perkin–Elmer TGA7 instrument. The analysis was conducted in the temperature range of 300–900 K in a nitrogen atmosphere under a constant flow rate of 20 ml.min^{-1}.

Differential scanning calorimetry (DSC) measurements at low temperature were carried out using a Perkin-Elmer DSC7 calorimeter in the temperature range from 120 K to 300 K at a heating rate of 10 K.min^{-1} using a polycrystalline sample in a flowing nitrogen atmosphere.

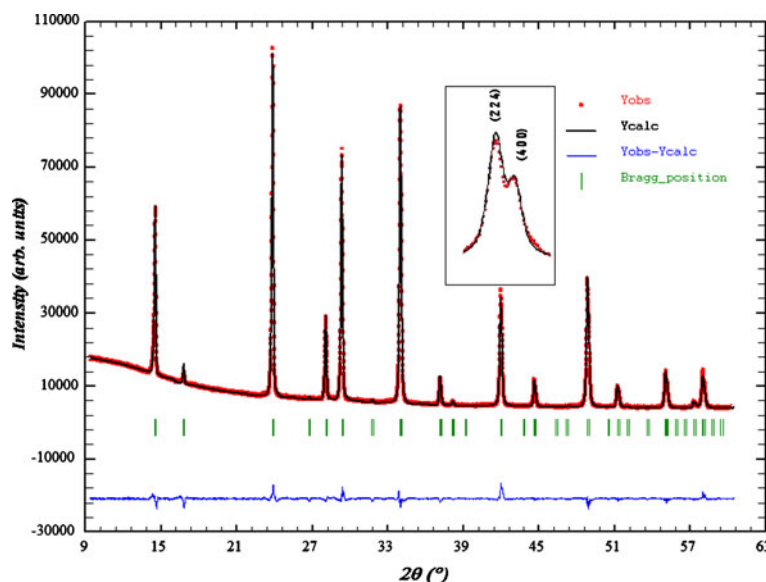## 2.4 *Spectroscopy analysis*

The spectroscopy FTIR at room temperature was used to confirm the presence of the different vibration mode of ammonium ion in our compound. KBr pellets containing the new sample was prepared and the FTIR spectra recorded using a Perkin-Elmer 1750 spectrophotometer.
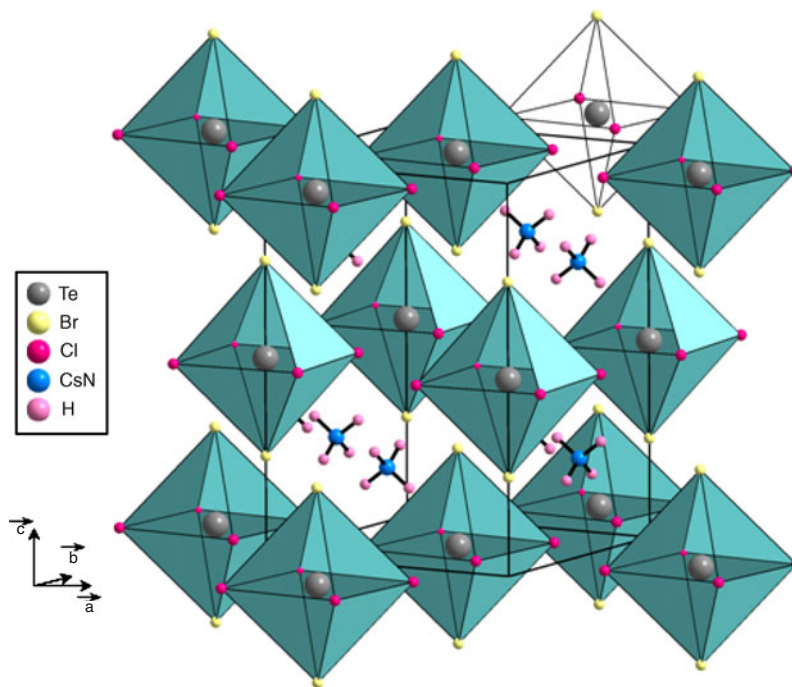
To complete the results of thermal behaviour and the FTIR spectroscopy, the new mixed compound was analysed by Raman spectra at different temperatures. Raman spectra of sample in sealed glass cell (2 mm in diameter), were obtained between 120 K and 450 K with a Horibo Jobin Yvan HR800 microcomputer system instrument using a conventional scanning Raman instrument equipped with a Spex 1403 double monochromator (with a pair of 600 grooves/mm gratings) and a Hamamatsu 928 photomultiplier detector. The excitation radiation was provided by coherent radiation with an He–Neon laser at a wavelength of 633 nm, and the output laser power was 50 mW. The spectral resolution, in terms of slit width, varied from 3 to 1 cm^{-1}.

3. Results and discussion

3.1 *Structure description*

The crystal structures of the A_2BX_6 usually belong to the large family of K_2PtCl_6 (the so-called antifluorite structure). For a tetragonally distorted K_2PtCl_6
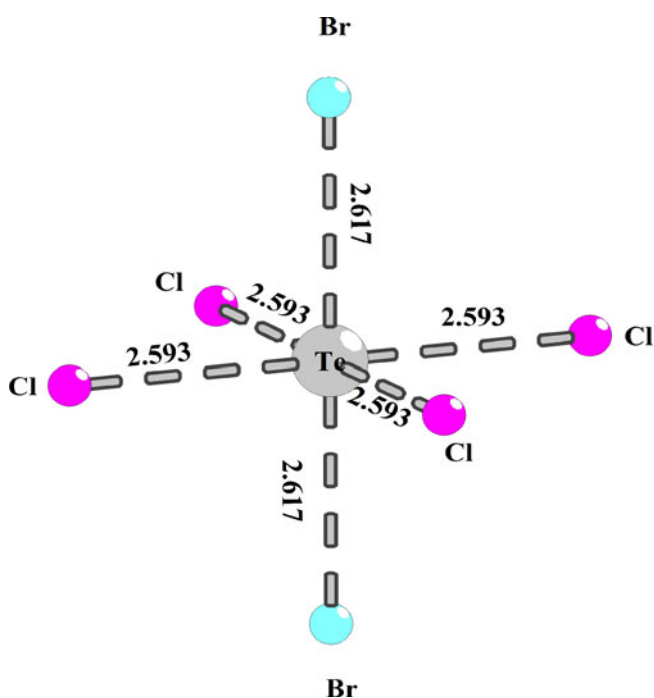

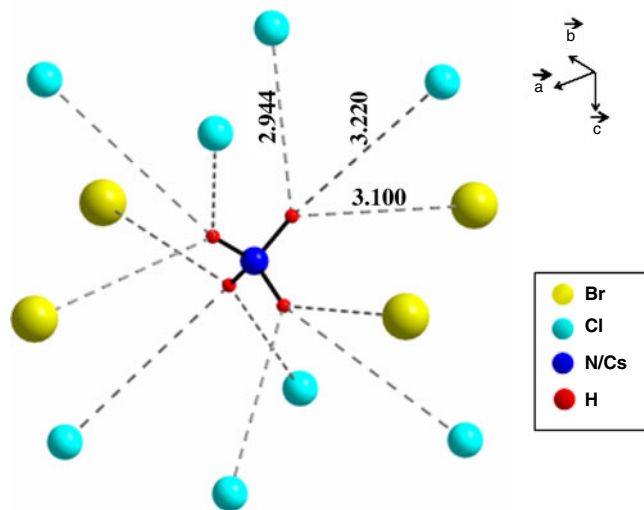**Figure 1.** X-ray powder diffraction pattern and refinement of $[Cs_{0.92}(NH_4)_{0.08}]_2TeCl_4Br_2$.

Figure 2. The structure of $[Cs_{0.92}(NH_4)_{0.08}]_2TeCl_4Br_2$.

type structure the space group P4/mnc was first proposed by Das and Brown, reporting a low temperature phase of $(NH_4)_2TeBr_6$.[16] In the present work, $[Cs_{0.92}(Nh_4)_{0.08}]_2TeCl_4Br_2$ crystallizes in the tetragonal space group (P4/mnc) with a = 7.452(1) Å, c =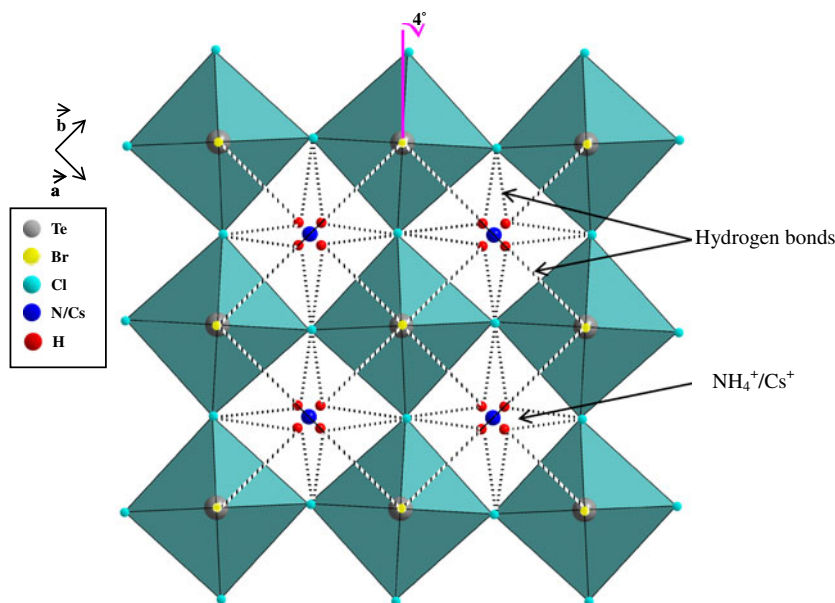 10.544(3) Å, at room temperature. The Te atoms lie on the 2(b) sites surrounded by an octahedron of chlorine and bromine) atoms in the 4(e) positions with coordinates (0, 0, z) and z = 0.25179(11) for Br and in the 8(h) positions with coordinates (x, y, 0) and x = 0.7640(3), y = 0.27337(8) for Cl. The Cs or N atoms occupy the 4(d) (0, 1/2, 1/4) sites, as shown in figure 2. The cohesion of the atomic arrangement is ensured by hydrogen and ionic bonding (N–H...Cl/Br and Cs^+–Cl^-/Br^-).

Figure 3. Tellurium environment in $[Cs_{0.92}(NH_4)_{0.08}]_2$ $TeCl_4Br_2$.

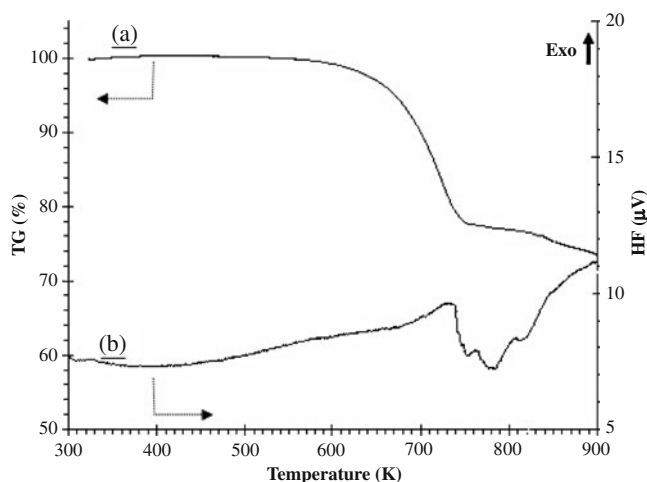**Figure 4.** Ammonium environment with the different possibility of hydrogen bond in $[Cs_{0.92}(NH_4)_{0.08}]_2TeCl_4Br_2$.

Figure 5. Projection along the four-fold axis with an anti-ferrorotative displacement of the $[TeCl_4Br_2]^{2-}$ octahedral: Show the hydrogen bond in compound $[Cs_{0.92}(NH_4)_{0.08}]_2TeCl_4Br_2$.

Each Te atom is surrounded by four chlorine and two bromine atoms forming a slightly distorted octahedron with distances Te–Cl is 2.596(12) Å and Te–Br is 2.617(15) Å (figure 3). The small differences of Te–Br and Te–Cl bond lengths in the mixed compound are not significant considering the standard deviations and are typical for a tetragonal refinement of positional parameters. So the point symmetry of the $Te(Cl_4/Br_2)^{2-}$ ion is still m3m. There appears to be no stereochemical active lone pair of electrons at Te (IV) in this hexahalogeno complex ion.
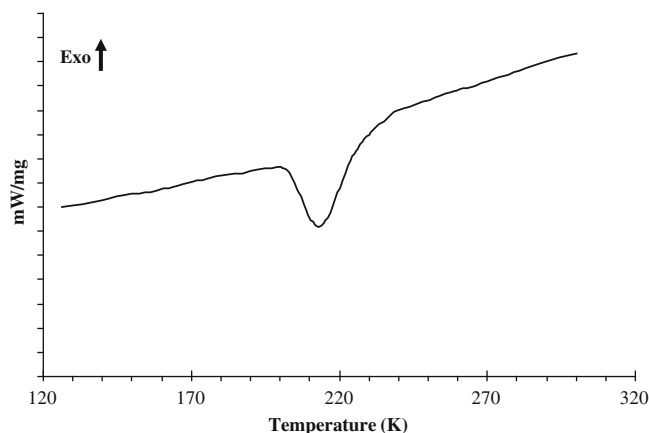
We note, that for $[Cs_{0.92}(NH_4)_{0.08}]_2TeCl_4Br_2$, the Te–Br distances vary, at most 0.064 Å from $(NH_4)_2TeBr_6$ [16]

structure to 0.078 Å from Cs_2TeBr_6 [7] structure and the Te–Cl distances vary, at less 0.015 Å from $(NH_4)_2TeCl_6$ [17] structure to 0.085 Å from Cs_2TeCl_6 [18] structure.

For $[Cs_{0.92}(NH_4)_{0.08}]_2TeCl_4Br_2$, in the tetragonal structure each monovalent cation (Cs^+/NH_4^+) is coordinated by 12 anions (figure 4): 8 Cl atoms at distances ranging from 3.621(7) Å to 3.836(6) Å and 4 Br atoms at distances equal to 3.728(4) Å. The Cs^+/NH_4^+ groups are located between the $TeCl_4Br_2$ octahedra ensuring the stability of the structure by ionic and hydrogen bonding contacts (Cs^+)—Cl^-/Br^- and N–H—-Cl/Br, respectively.

Figure 6. (a): Thermogravimetric (TG) and (b): differential thermal analysis (DTA) of $[Cs_{0.92}(NH_4)_{0.08}]_2TeCl_4Br_2$.

Figure 7. DSC thermogram of $[Cs_{0.92}(NH_4)_{0.08}]_2TeCl_4Br_2$ in the temperature range of 120 to 320 K.

The hydrogen atoms were located geometrically in the site symmetry 4/m. All the hydrogen atoms of NH_4^+ are involved with the atoms of bromine and chlorine octahedra ($TeBr_2Cl_4$) to form a three-dimensional network of hydrogen bonds with the ionic cohesion of the crystal lattice (figure 5). The Br atom enters into hydrogen bond H....Br with distance equal to 3.100 (6) Å. But, the H bond length H...Cl is in the order of 2.944(18) Å (figure 4). The difference in length of bond is the origin of the strong interaction H...Cl compared to that of H...Br due to the difference of the electronegativity between chlorine and bromine atoms.

3.2 *Thermal analysis*

Figure 6 presents the typical TG/DTA curves measured at a heating rate of 10 K.min^{-1}. The DTA curve, obtained over a temperature range of 300–900 K, illustrates that there are a large endothermic process pointed at 780 K. As is indicated by the TG curve, this peak is accompanied with a loss mass, implicating the decomposition of sample.

At low temperature, a transition from phase I to phase II was detected at 213 K by DSC (figure 7). This transition can be attributed to an order–disorder phase transition involving the hydrogen bonds coupled with the distortion of the octahedral. This result has been confirmed by Raman studies.

3.3 *Spectroscopic studies*

Raman and IR spectroscopy at room temperature were used to determine the different observed bands of the mixed compound $[Cs_{0.92}(NH_4)_{0.08}]_2TeCl_4Br_2$ and to confirm the tellurium coordination.

The FTIR spectral data and the band assignments of $[Cs_{0.92}(NH_4)_{0.08}]_2TeCl_4Br_2$ at room temperature are presented in table 4, respectively. The intense absorption bands, at 3131 cm^{-1} and 1402 cm^{-1} are attributed to the triply degenerate vibrations, υ_3 (stretching) and υ_4 (deformation), respectively. The

Table 4. Observed IR frequencies (cm^{-1}) and band assignments for $[Cs_{0.92}(NH_4)_{0.08}]_2TeCl_4Br_2$ at room temperature.

Frequencies (cm^{-1})	Assignments
1402 vs	υ_4 (NH$_4$) (Deformation)
1606 s	υ_2 (NH$_4$) (Deformation)
2823 vw	$2\upsilon_4$ (NH$_4$)
3012 w	$\upsilon_2 + \upsilon_4$ (NH$_4$)
3131 vs	υ_3 (NH$_4$) (Stretching)

Relative intensities: vs, very strong; s, strong; w, weak; vw, very weak.

band at 1606 cm^{-1} corresponds to υ_2 deformation mode. Other bands corresponding to interactions between these fundamental vibrations (i.e., overtones and combination bands) are observed at 3012 cm^{-1} ($\upsilon_2 + \upsilon_4$) and 2823 cm^{-1} ($2\upsilon_4$).[19]

At room temperature, the Raman spectrum of the mixed compound $[Cs_{0.92}(NH_4)_{0.08}]_2TeCl_4Br_2$ is quite resolved, which confirms the presence of the polar phase. The structure of the $[Cs_{0.92}(NH_4)_{0.08}]_2TeCl_4Br_2$ is characterized by the existence of the octahedral TeX_6^{2-} anions (X: Cl/Br), The interesting feature of the new mixed compound is the coexistence of two types of bands corresponding to the vibrational modes of Te–Cl and Te–Br. The ordering of these two modes of vibrations as well as the dynamics of the NH_4^+ groups determines the properties of this sample.

Figure 8 presents the Raman spectra of the $[Cs_{0.92}(NH_4)_{0.08}]_2TeCl_4Br_2$ sample. By comparing with pure compounds,[18] the Raman spectra can be divided into different spectral frequency ranges and lines: from 210–310 cm^{-1} the bands can be assigned to the Te–Cl stretching modes (υ_1 and υ_2), the range from 170 to 210 cm^{-1} can be assigned to symmetric Te–Br stretching vibrations (υ_1 and υ_2) and the Raman lines observed at 131 cm^{-1} and 160 cm^{-1} are associated respectively to Te–Br and Te–Cl bending vibration (υ_5). The line observed at 115 cm^{-1} is attributed to the liberations mode of NH_4^+ and the range from 50 to 100 cm^{-1} can be attributed to the presence of the translation modes of Cs^+ and NH_4^+.

In the present work, we would like to concentrate on thermal changes of the frequencies of symmetrical bending vibrations of the Te–Cl (intense band at 130 cm^{-1} accompanied with a broad band at 127 cm^{-1}) and the symmetric bending vibrations of Te–Br (at 160 cm^{-1}) as well as frequencies of liberations and translation modes of NH_4^+ (band at 115 cm^{-1} and 91 cm^{-1}, respectively).

By increasing temperature, the sample passes from phase I to phase II. In fact, as one can see the Raman spectra change significantly at T = 213 K. Below this temperature the Raman lines which are related to υ_5 Te–Cl vibrations split into two well-developed distinct lines ($\sim$ 127 and 130 cm^{-1}). The lines which are assigned to υ_5 Te–Br vibration ($\sim$ 160 cm^{-1}) do not exhibit changes in their shape but the positions of this bands undergo significant changes at T = 213 K. The bands relative to υ_1 (TeCl), at 285, 277 and 268 cm^{-1} decrease in intensity on raising the temperature and the last one at 268 cm^{-1} disappears after the phase transition detected by DSC at 213 K. On the other hand, the υ_2 (TeCl) bands which appear at 245 and 235 cm^{-1} decrease in intensity and becomes very broad. The bands at

Figure 8. Raman spectra of $[Cs_{0.92}(NH_4)_{0.08}]_2TeCl_4Br_2$ at different temperatures.

$91\,cm^{-1}$, $60\,cm^{-1}$ and $188\,cm^{-1}$ decrease in intensity and broaden as the temperature is increased. Other than this, the peak observed at $115\,cm^{-1}$ decreases in intensity on raising the temperature and disappears after the temperature $T = 213\,K$, indicate the large dynamic motion of NH_4^+ at phase II.

4. Conclusion

The results of detailed XRD, low temperature Raman and DSC studies of the new substituted $[Cs_{0.92}(NH_4)_{0.08}]_2TeCl_4Br_2$ are presented. The title compound crystallises in P4/mnc tetragonal space group. The main feature of the structure of this material is based on isolated TeX_6 (X = Cl or Br) octahedra connected by ionic and hydrogen bonding through the Cs or N atoms which are located between the octahedral TeX_6 units ensuring the stability of the structure. The Raman spectra (50–$350\,cm^{-1}$) of powder sample was studied

at temperature ranging from 120 to 400 K. The thermal evolution of the Raman spectra reveals an order–disorder phase transition at about 213 K involving the hydrogen bonds coupled with the distortion of the octahedral. Moreover, DSC measurement in the temperature range (120–300 K) was also presented. The occurrence of a low-temperature phase transition near 213 K is well-evidenced.

Low temperature XRD and luminescence measurements investigations of the title compound are in our future study in order to confirm the nature of transformation observed by DSC and Raman and to know the influence of distortion of the Te(IV) coordination octahedron on its luminescence.

References

1. Gillespie R J and Nyholm R S 1957 *Quart. Rev.* **11** 339
2. Barrier N, Rueff J M, Lepetit M B, Contreras-Garcia J, Malo S and Raveau B 2009 *Solid State Sci.* **11** 289

3. Zhang S, Huang Y, Shi L, Qiao X and Seo H J 2009 *Physica B.* **404** 4136
4. Gaitan M, Jerez A, Pico C and Veiga M L 1987 *Mat. Res. Bull.* **22(4)** 477
5. Loukil M, Ben Salah A and Kabadou A 2010 *J. Alloys Compd.* **L10** 488
6. Brown I D 1964 *Canad. J. Chem.* **42** 2758
7. Das A K and Brown I D 1966 *Canad. J. Chem.* **44** 939
8. Berg R W and Nielsen K 1979 *Acta Chem. Stand.* **A33** 157
9. Abriel W 1982 Z. *Kristallogr.* **1** 159
10. Louër D and Louër M 1972 *J. Appl. Crystallogr.* **5** 271
11. Boultif A and Louër D 2004 *J. Appl. Crystallogr.* **37** 724
12. Rietveld H M 1969 *J. Appl. Crystallogr.* **2** 65
13. Rodriguez-Carjaval 1990 *J. Proceedings of the satellite meeting on powder diffraction* **127**
14. Young R A and Wiles D B 1982 *J. Appl. Crystallogr.* **15** 430
15. Roisnel T 2001 *Fullprof Rietveld-Juan Rodriguez-Carvajal and Win-Plotr Interface.*
16. Das A K and Brown I D 1969 *Canad. J. Chem.* **47** 4288
17. Nakamoto K 1963 *Infrared spectra of inorganic, coordination compounds* (New York; Singapore: Wiley)
18. Berg R W, Poulsen FW and Bjerrum N J 1977 *J. Chem. Phys.* **67(5)** 1829
19. Engel G 1933 *Naturwissenschaften* **21** 704
20. Williams L R and Haskett P 1969 *Anal. Chem.* **41** 1138